Available online at www.sciencedirect.com
ScienceDirect
Computational Materials Science 42 (2008) 570–578
COMPUTATIONAL MATERIALS SCIENCE
www.elsevier.com/locate/commatsci

Simulation of the strain rate sensitive flow behavior of SiC-particulate reinforced aluminum metal matrix composites

İsmail Tirtom [a,e,*], Mustafa Güden [a,b,c], Hasan Yıldız [d]

[a] Materials Science and Engineering, İzmir Institute of Technology, Urla, İzmir 35430, Turkey
[b] Mechanical Engineering, İzmir Institute of Technology, Urla, İzmir 35430, Turkey
[c] Center for Materials Research, İzmir Institute of Technology, Urla, İzmir 35430, Turkey
[d] Mechanical Engineering Department, Ege University, Bornava, İzmir 35040, Turkey
[e] Graduate School of Engineering, Mechanical Systems and Design, Tohoku University, Sendai 980 8579, Japan

Received 1 June 2007; received in revised form 1 September 2007; accepted 10 September 2007
Available online 25 October 2007

Abstract

Strain rate dependent compression mechanical behavior of an SiC-particulate reinforced Al (2024-O) metal matrix composite (MMC) with different particle volume fractions was numerically investigated at various strain rates. Calculations were performed using axisymmetric finite element unit cell model, in which an elastic SiC particle was embedded inside a strain rate sensitive viscoplastic Al matrix. Stress–strain curves of Al matrix material were derived from Split Hopkinson Pressure Bar experiments at various strain rates and used as inputs in the FEM model. Numerically computed stress–strain curves and strain rate sensitivity were compared with those of experiments for a 15% SiC-particulate reinforced MMC. Computed strain rate sensitivity of the MMC was found to be higher than that of the matrix alloy and increased with increasing strain contrary to the strain independent matrix strain rate sensitivity. The strain rate sensitivity of the MMC was also found to increase with increasing particle volume fraction at the same particle size. Finally, several possible reasons including assumptions used in the model, adiabatic heating, microstructural variations between the composite matrix and matrix alloy, particle shape and distribution and damage accumulation for the small discrepancy found between computed and experimental stress–strain curves and strain rate sensitivity of the composite were discussed.
© 2007 Elsevier B.V. All rights reserved.

PACS: 81.05.Ni; 81.70.Bt; 47.11.Fg

Keywords: Metal matrix composite; Particulate; FEM; Strain rate sensitivity

1. Introduction

Metal matrix composites (MMCs) exhibit a significant improvement in mechanical performance over monolithic alloys. Some specific advantages include high specific modulus and strength, high strength/weight ratio and high corrosion and temperature resistance [1]. High strain rate mechanical properties of these materials are important in applications where sudden increase in loading can occur. These include the impact of foreign objects to structural components, collisions of the parts, projectile-armor interactions and metal forming processes such as extrusion and forging.

Many experimental studies have been conducted to determine quasi-static mechanical properties of particle, whisker and long and short fiber reinforced MMCs and their properties have been well characterized [2–6]. In parallel with experimental studies, theoretical and numerical investigations have been performed to predict the stiffness and the strength of the composites, given the mechanical properties of the matrix and reinforcement phases [7–10].

* Corresponding author. Address: Graduate School of Engineering, Mechanical Systems and Design, Tohoku University, Sendai 980 8579, Japan.
E-mail address: itirtom@gmail.com (İ. Tirtom).

0927-0256/$ - see front matter © 2007 Elsevier B.V. All rights reserved.
doi:10.1016/j.commatsci.2007.09.005

The parameters widely studied include reinforcement volume fraction, size, shape, aspect ratio and distribution [7,10–12].

The mechanical properties under high strain rates have not been investigated and developed as much. To our knowledge the first experimental investigation of high strain rate behavior of MMCs is due to Harding and Taya [13] and Marchand et al. [14]. Studies of the high strain rate behavior of specific MMCs include those of Perng et al. [15], Hong and Gray [16], Yadav et al. [17], Chichili and Ramesh [18] and Guden and Hall [19]. A higher strain rate sensitivity of the composite compared with matrix material has been generally found in these studies. Yadav et al. [17] numerically showed that the effect of strain rate in particulate reinforced MMCs would be strongly dependent on the particle volume fraction. Bao and Lin [10] and Yadav et al. [17], based on axisymmetric unit cell model, showed that the effect of strain rate is coupled with the particle volume fraction and the strain rate hardening of the composite might be significantly higher than that of the matrix due to the constraining effect of particles. Li and Ramesh [7] also studied the effects of particle shape and aspect ratio on the high strain rate response of SiC-particulate (SiC_p) reinforced Al MMCs, and concluded that both variables have a strong influence on the flow stress at high strain rates.

This study presents a computational investigation of the compression stress–strain behavior of an SiC_p reinforced Aluminum (2024-O) MMC, with different particle volume fractions, over a wide range of strain rate from quasi-static ($\sim 10^{-3}\ s^{-1}$) to high strain rates ($\sim 10^{4}\ s^{-1}$). The model applied however uses experimentally determined stress–strain behavior of the unreinforced matrix alloy determined at different strain rates. Axisymmetric unit cell models with two different boundary conditions were implemented in LUSAS finite element model (FEM) program, considering the composite as a viscoplastic matrix embedded with strain rate insensitive rigid ceramic particles. The numerical results of the models were also compared with the experimental results in order to validate the model capability for predicting the stress–strain curves (at different strain rates) and strain rate sensitivity of the similar MMCs.

2. Model description

2.1. Unit cell model

2.1.1. Geometry and model properties

The modelling was based on the widely used axisymmetric unit cell model, which represented the overall mechanical behavior of the particulate reinforced MMC (Fig. 1). Due to symmetry, only one quarter of the axisymmetric unit cell was used in the calculations (Fig. 1c). SiC particles were assumed spherical, elastic and homogeneously dispersed in the matrix. The elastic modulus and Poisson's ratio of SiC were taken 450 GPa and 0.17, respectively. A perfect bonding between particle and matrix was assumed (no particle cracking and interface sliding). The particles and matrix remained undamaged during the course of deformation. Similar models are found in [7,8]. The geometrical parameters of the used model (particle radius, *r,* and unit cell cylinder radius, *R*) are shown in Fig. 1c. The effect of reinforcement volume fraction on the stress–strain behavior of the model composite (SiC_p/2024-O Al MMC) was investigated using the unit cell models containing 10, 15 and 25 volume percentages of SiC_p (Fig. 2a–c). The particle size was taken constant, 30 μm.

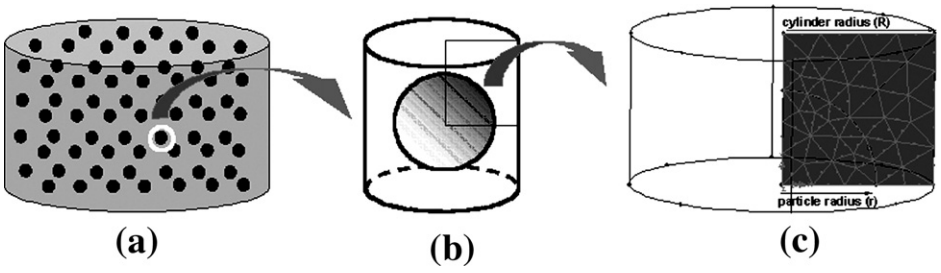

Fig. 1. Schematic of the model: (a) composite, (b) unit cell and (c) axisymmetric unit cell model.

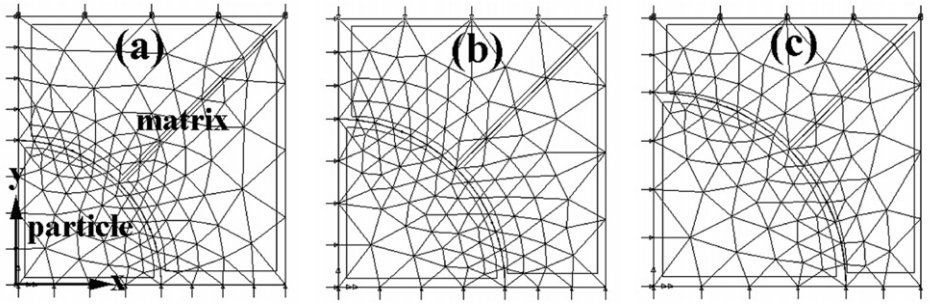

Fig. 2. Unit cell composite models: (a) 10, (b) 15 and (c) 25% SiC particles (particle radius is constant and 15μm).

2.1.2. FEM settings

LUSAS 6 noded triangle (TAX6), 2D continuum axisymmetric solid elements with quadratic shape functions were used for irregular meshing of the axisymmetric unit cell models [20]. Initially, 150 (450 Gauss points) and 206 (618 Gauss points) fully integrated elements were investigated in the models. It was found that the stress values for a 15% particulate reinforced MMC at a constant strain of 15% show only about 1% difference between two numbers of elements; therefore the modeling continued with 206 fully integrated elements. Because of the symmetry, the left and bottom edges of the unit cell were fixed in the x ($dx = 0$) and y ($dy = 0$) directions. Top edge was constrained in the y-direction as it remained straight after loading for geometrical fitting. Right edge of the unit cell was free to move in x direction [7]. The computations for various particle volume fractions were performed.

2.1.3. Loading

Uniaxial compression loading of the unit cell was performed by imposing two different incremental displacements in the y direction: 0.002% incremental strain until 1% strain and 1% incremental strain after 1% strain. The deformation of the composite was modeled using von-Misses theory of plastic flow. The compressive flow stress–strain data of the matrix alloy at the specific average strain rate of the composite studied was entered to the program. Stress–strain curves of Al matrix material was derived from Split Hopkinson Pressure Bar experiments at various strain rates.

2.1.4. Post-processing

The macroscopic true stress was calculated using the following equation;

$$\sigma_{ci} = \frac{\sum_{j=1}^{N} \sigma_j}{N} \tag{1}$$

where, σ_{ci} is the average composite stress at ith increment (loading step), σ_j is the element stress at the Gauss points and N is the total number of Gauss points. Macroscopic true strain was calculated using the following relation,

$$\varepsilon_{ci} = \ln\left(\frac{l_i}{l_o}\right) \tag{2}$$

where, ε is the strain and l and l_o are the final and the initial length of the unit cell in the y direction, respectively.

2.2. Model composite

The modeling results of the compressive stress–strain curves of the composite were compared with those of 15% SiC_p reinforced 2024-O Al MMC. The composite was manufactured by stir casting and the microstructure of the composite is shown in Fig. 3. The average particle size was 30 μm, but the particle size ranged between 10 and 50 μm. The average matrix grain size was 200 μm. Since the particles were pushed by the growing dendrites, they were collected at the grain boundaries (Fig. 3). The unreinforced matrix alloy was an extruded and cross-rolled wrought alloy. Solution treatment was applied to the alloy in order to obtain cast matrix alloy properties. The heat treatment process was conducted at 385 °C for 3 h followed by cooling to 260 °C (28 °C/h) and cooling in the furnace to room temperature.

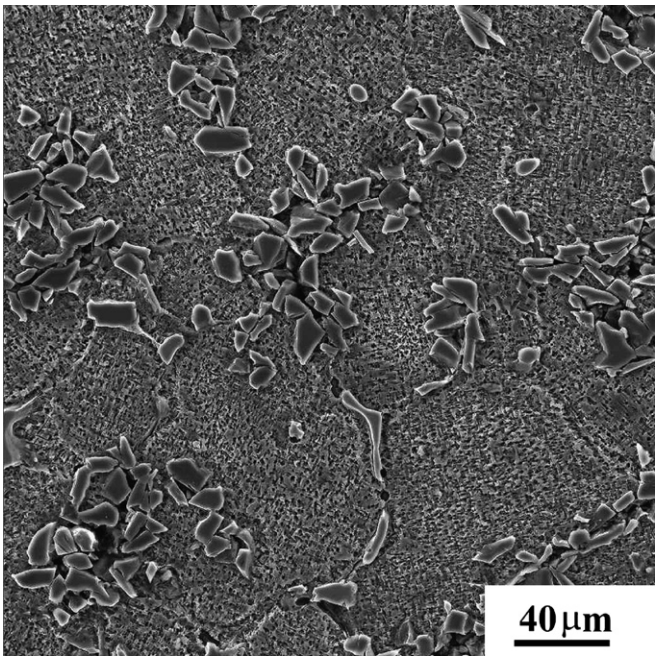

Fig. 3. SEM micrograph of SiC_p reinforced 2024 Al-O, showing the particle clustering at grain boundaries [19].

The composite and matrix alloy quasi-static and dynamic compression behavior was previously investigated by Güden and Hall [19] using Instron and Split Hopkinson Pressure Bar (SHPB) techniques in the strain rate range of $\sim 10^{-4}$–3000 s^{-1}. The constitutive equation of the matrix alloy was determined by fitting the flow stresses (at 6% strain)–strain rate data (Fig. 4) with the following linear hardening equation:

$$\sigma_D = \sigma_S + K\dot{\varepsilon} \tag{3}$$

where, σ_D and σ_S are the dynamic and reference strain rate flow stresses, respectively and K is the strain rate sensitivity factor. The reference strain rate was chosen 1.5×10^{-3} s^{-1}, corresponding to the quasi-static strain rates. Linear fitting to the data in Fig. 4 results in a matrix strain rate sensitivity (K) value of 0.014929. Fig. 5 shows the computed stress–strain curves of the matrix at various strain rates, based on Eq. (3), and comparison between experimental and computed stress–strain curves at 1140 and 3200 s^{-1}. A good agreement between calculated and experimental stress–strain curves in this figure confers that matrix constitutive equation can be simply presented by the Eq. (3). The

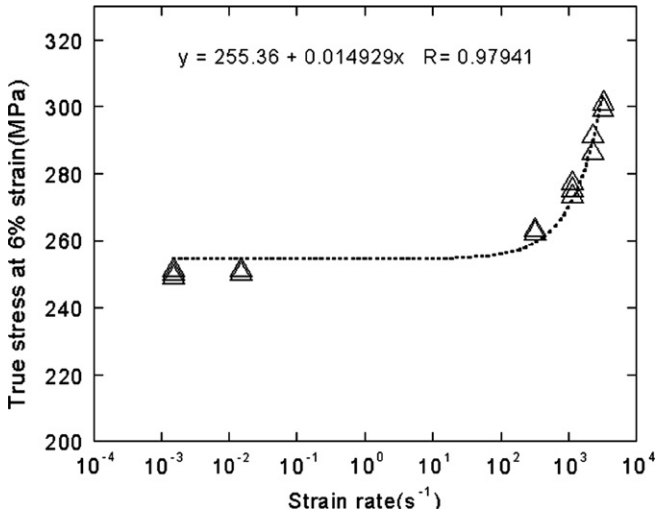

Fig. 4. Variation of matrix flow stress at 6% strain with strain rate.

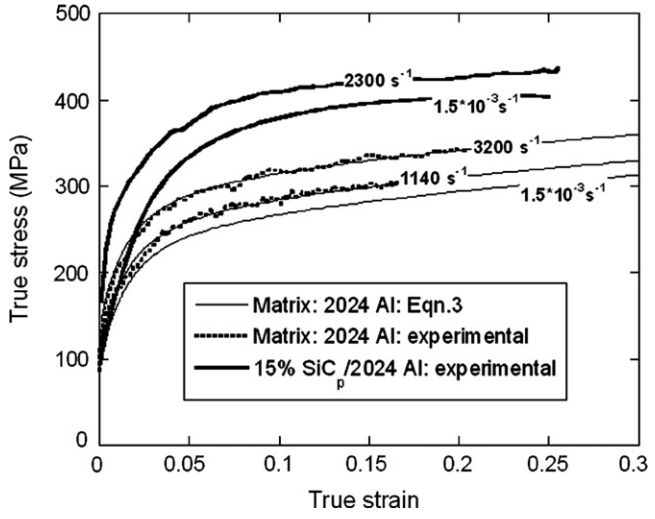

Fig. 5. Calculated and experimental stress–strain curves of the matrix and experimental stress–strain curves of the composite at various strain rates.

effect of strain rate on the compression behavior of the 15% SiC_p reinforced composite is also shown in Fig. 5. The increasing flow stress of the composite with increasing strain rate from quasi-static to high strain rates in this figure shows a strain rate sensitive flow stress behavior of the composite.

3. Results

Numerically computed stress–strain curves of the model and experimental stress–strain curve of the 15% SiC_p reinforced MMC at 1.5×10^{-3} s^{-1} are shown in Fig. 6. A similar behavior was also previously found in the modeling of cylindrical and spheroidal particle reinforced MMC [7]. It is also noted in Fig. 6 that the model predicts the composite stress–strain behavior reasonably well until about 0.15 strain compared with experimental results.

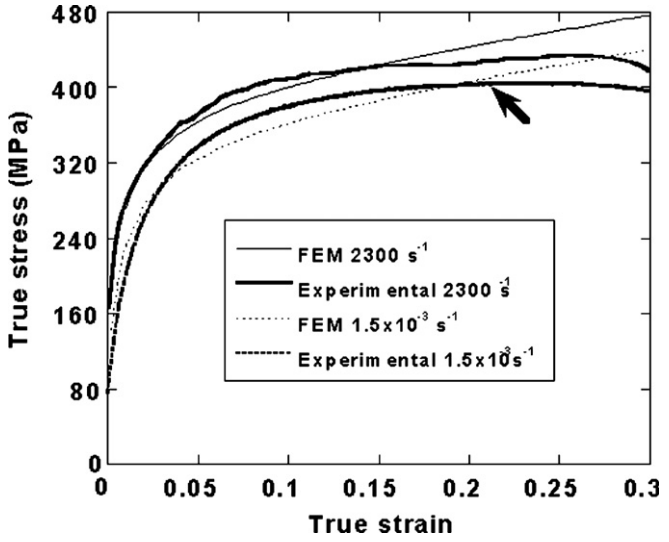

Fig. 6. Comparison of FEM and experimental stress–strain curves of the 15% SiCp 2024-O MMC at 1.5×10^{-3} and 2300 s^{-1} strain rates.

The effect of particle volume fraction on the stress–strain behavior of the composite at quasi-static strain rate is shown in Fig. 7. As seen in this figure, increase in reinforcement volume fraction at a constant particle size (30 μm) increases both flow stresses and strain hardening rate of the composite.

Computed composite flow stress–strain behaviour of the MMC at quasi-static and high strain rates are shown sequentially in Figs. 8 and 9 for 10% and 25% particle reinforcements. The flow stresses corresponding to 5% strain were extracted from these curves and shown as function of strain rate in Fig. 10 for 10%, 15% and 25% particle volume fractions. Linear interpolation to the data in this figure gives the strain rate sensitivity of the composite. Figs. 11 and 12 show the variation of the K values as functions strain and volume percentage of the particles, respectively.

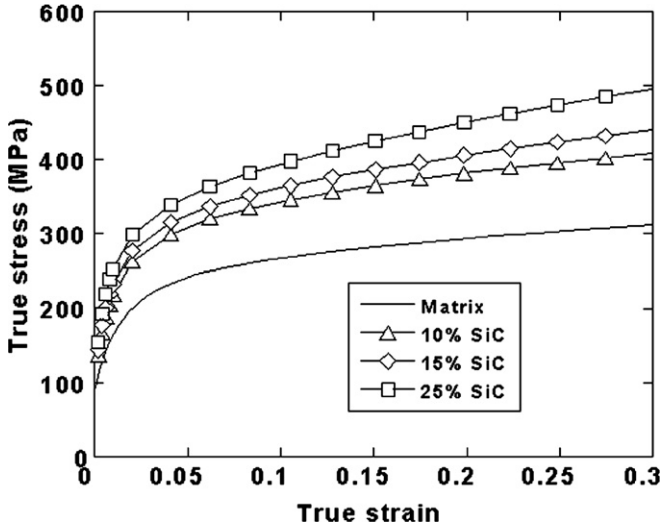

Fig. 7. FEM stress–strain curves of unit cell models of composite with various volume percentages of SiC particles at 1.5×10^{-3} s^{-1}.

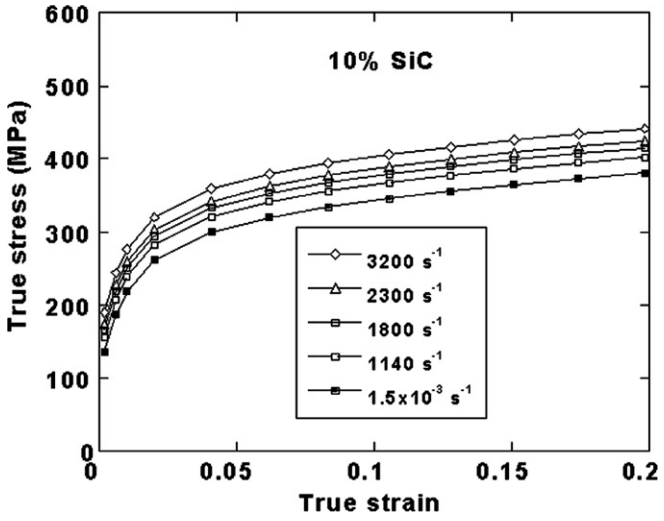

Fig. 8. FEM stress–strain curves of 10% SiC_p unit cell model of composite at different strain rate.

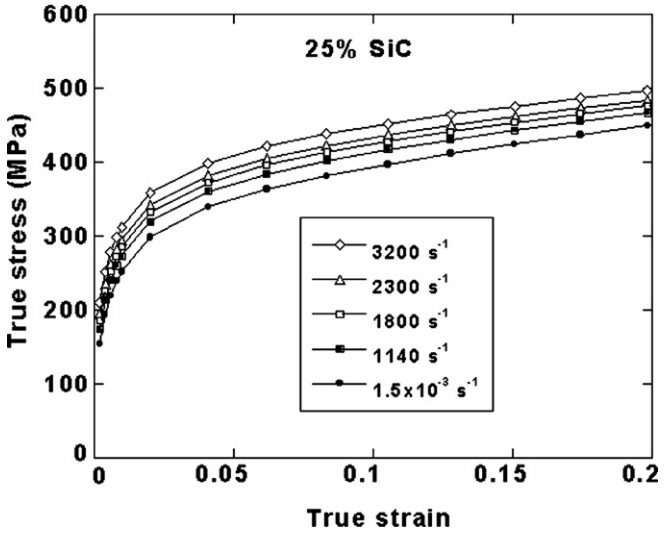

Fig. 9. FEM stress–strain curves of 25% SiC_p unit cell model of composite at different strain rate.

The highest K value at 5% strain is found in 25% SiC_p volume fraction (0.02007) and the smallest in 10% SiC_p reinforced composite (0.018139). The rate sensitivity of the matrix alloy (0.0149) is smaller than that of the composite, as shown in Fig. 11. Contrary to the assumed strain independent matrix alloy rate sensitivity, composite rate sensitivity also increases with increasing strain (Fig. 12).

The experimental and computed K and σ_S values of Eq. (3) are tabulated in Table 1 for 15% SiC_p 2024-O Al composite. For unit cell models, the rate sensitivity of the composite is higher than the matrix alloy and experimental composite strain rate sensitivities.

4. Discussion

The effect of strain rate on the flow stresses of the FCC and BCC materials is well documented. Tirupataiah and

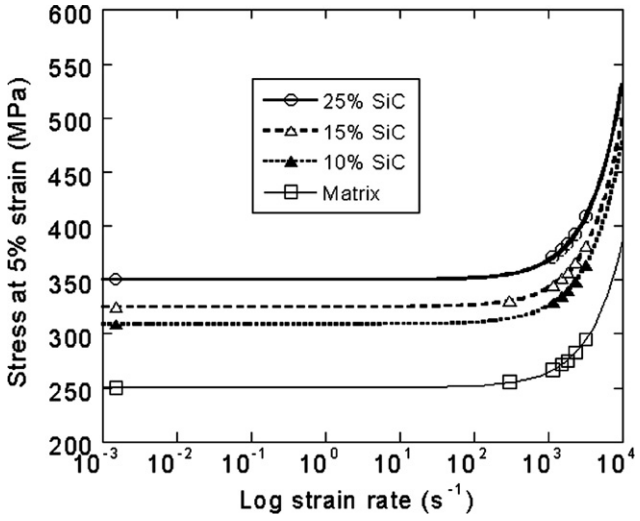

Fig. 10. Variation of the flow stress of the composite (5% strain) with strain rate.

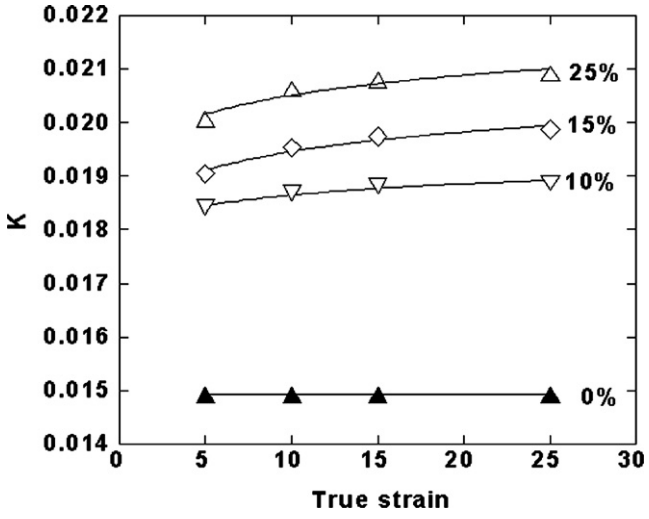

Fig. 11. K *vs.* strain curves of the composite at $1.5 \times 10^{-3}\ s^{-1}$.

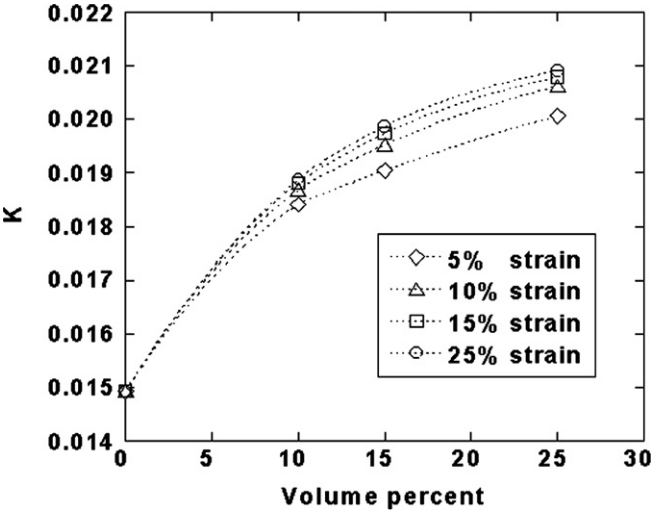

Fig. 12. K *vs.* volume percentage of the particles at $1.5 \times 10^{-3}\ s^{-1}$.

Table 1
Parameters of Eq. (3) as function of strain; experimental and unit cell models

Strain (%)	MMC experimental		MMC (unit cell model)	
	σ_S (MPa)	K	σ_S (MPa)	K
10	378.9	0.01475	426.3	0.02310
15	390.7	0.01550	456.7	0.02367
25	344.9	0.01390	483.8	0.02398

Sundararajan [21] have represented flow stress *vs.* logarithm of strain rate in two parts, a high strain rate sensitive regime after a transition strain rate and a lower strain rate regime below the transition strain rate. Tirupataiah [22] has further constructed the transition strain rates for a number of metals and showed that the transition strain rate for common metals and alloys lies between 102 and 104 s^{-1}. Before the transition strain rate, it is usually assumed that the deformation is controlled by the thermally activated deformation mechanism [23] and a logarithmic relation between stress and strain rate is usually found in this regime as,

$$\sigma_D = \sigma_S + K \log \dot{\varepsilon} \tag{4}$$

Above the transition strain rate, the flow stress is assumed to be drag controlled [23]. Stress and strain rate in this regime is linear and expressed by Eq. (3).

In order to apply Eqs. (3) and (4) to the flow stresses, the experimental flow stress data between quasi-static and high strain rates, 1 and 100 s^{-1}, must also be provided. Using conventional static and dynamic testing methods, the experimentation within this strain rate regime could not be possible. However, the matrix flow stresses of the studied composite material are sufficiently well represented by Eq. (3) within the studied strain rate regime.

The agreement between the unit cell model and experimental stress–strain curves for the 15% particle reinforced MMCs is reasonably good, although the latter shows slightly higher flow stresses before 15% strain (Fig. 6). At lower strains, below 5%, high strain rate flow stress data of SHPB testing however do not show exact material property. This is because at least four stress wave reversals are required in SHPB for stress homogenization in the sample, which may occur approximately within 1–4 μs (0–10% strain) depending on tested sample wave velocity and size and applied strain rate [24]. At lower strain rates, for small size samples, stress homogenization occurs at lower strain levels. One can therefore tempt to use flow stresses obtained at lower strain rates for the representative material property. However, the lower the strain rate is, the smaller the final strain attained is in the sample and therefore; comparison of the relatively lower and higher strain rate flow stresses at larger strain levels is not possible.

It is also noted in Fig. 6 that while numerical flow stresses increase continuously with increasing strain, the experimental quasi-static and high strain rate flow stresses showed a reduced work hardening after approximately 15% strain. This was most likely due to the damage accumulation in the composite at larger strains and at around 30% strain, the composite failed by forming shear bands, lining 45° to the load axis as shown in Fig. 13 for the composite sample tested until about 30% strain.

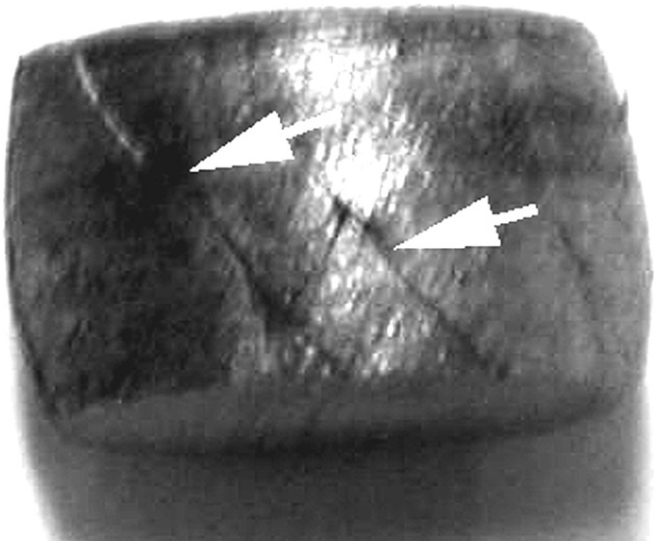

Fig. 13. Micrograph of the compressed (32% strain, 1.5×10^{-3} s^{-1}) MMC at quasi-static strain rate.

Increasing particle volume fraction has been found to have two major effects on the composite stress–strain behavior. These are (i) increase of the flow stress and (b) strain hardening rate. An increase in the volume fraction of the particle obviously increases the amount of load carried by the strong particles. The higher strain hardening behavior of the composite with the higher particle volume fractions is due to the development of the higher stresses as compared with the composite with lower particle volume fraction at the same average strain.

The increased strain sensitivity of the composite relative to the matrix alloy is due to the constraint effect of the particles [7,10]. This effect also increases with increasing particle volume fraction. The higher the particle volume fraction, the larger the maximum strain and hence the strain rate attained in the composite, leading to increased strain rate sensitivity. At an average strain rate, for example, the maximum strain rate in the matrix may rise well above the average strain rate. This forms a strengthening effect in the composite if the matrix flow stress is strain rate sensitive. Li and Ramesh [7] have previously proposed this explanation for the increased strain rate sensitivity in the particle reinforced MMCs. Similarly, since the matrix flow stress increases with increasing strain rate in the present model, the composite flow stress also increases but with an amount higher than the matrix flow stress at a constant strain.

The rate insensitive behavior of the ceramic materials has been observed in the strain rate regime of quasi-static to 100 s^{-1} [25]. Strain rate sensitive failure strength in ceramic materials has been found at strain rates higher than

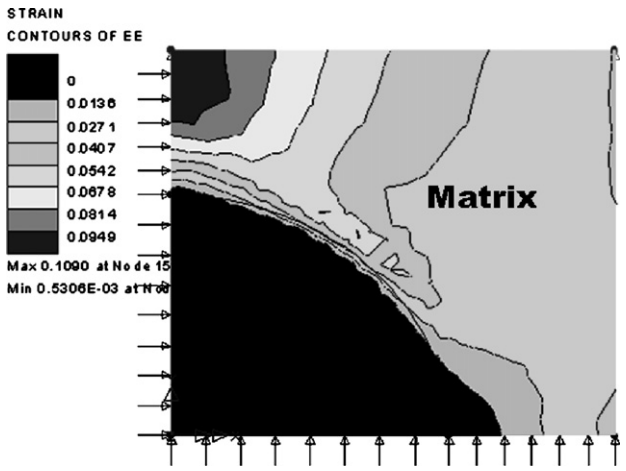

Fig. 14. Equivalent strain distribution at 0.02 average strain in 15% SiC_p composite at $1.5 \times 10^{-3}\ s^{-1}$.

$1000\ s^{-1}$ [25]. However such high strain rates could only be attained in the composite when the average strain rate in the composite would reach extremely high strain rates. Fig. 14 shows the distribution of the equivalent strain in the 15% SiC composite at an average strain of 0.02. The average strain in the particle is found less than 0.02, while the average strain of the matrix is higher than the average strain of the composite. This shows an average matrix and particle strain rates higher and lower than average composite strain rate, respectively. It should also be noted that the present model is based on the matrix stress–strain relation chosen at the average strain rate of the composite; this will in fact expected to increase the stress and strain rate sensitivity values of the composite further.

The discrepancy between experimental and numerical flow stresses and rate sensitivity of the composite might be also due to several complex factors. The discrepancy may partly be due to the experimental errors in the SHPB as explained previously. The errors in SHPB analysis mostly occur at low strains and therefore; could not be used to explain for the discrepancy at larger strains. One should also consider that the matrix microstructure in the composite might be quite different from that in monolithic alloy, although both have the same composition. Microscopic studies have shown that in particulate reinforced MMCs the matrix grain size is smaller than monolithic alloy produced by the same processing parameters and the precipitation reactions are also faster in the composite [26].

In metals, most of the plastic deformation work is converted into heat and the conversion factor is usually assumed 90–95%. Mason et al. [27] measured the rate of conversion of plastic work into heat in 2024 Al alloy at high strain rates. The conversion factor was found to reach 85–90% after about 10% strain, a result that is very similar to the predicted values. At high strain rates, the deformation is usually assumed to be adiabatic or near to the adiabatic condition due to short deformation duration for any significant heat dissipation [28]. Under adiabatic conditions, the temperature of the material rises as deformation proceeds and the increase of temperature is expressed as,

$$\Delta T = \frac{\psi}{C\rho}\int \sigma \mathrm{d}\varepsilon \tag{5}$$

where ΔT, C and ρ are the temperature increase, specific heat and density, respectively, and ψ is the conversion factor of plastic work into heat. The flow stress of most metals is quite sensitive to temperature [29] and, therefore, adiabatic heating can cause stress softening. The effect of stress softening due to adiabatic heating should be also taken into account for particularly strain rates above $100\ s^{-1}$. The critical strain rate for adiabatic strain rates is given as [30]

$$\dot{\varepsilon}_{cr} = \frac{4\alpha\varepsilon}{L^2} \tag{6}$$

where α is the thermal diffusivity and L is the specimen length. Using a thermal diffusivity of $5 \times 10^{-5}\ m^2\ s^{-1}$ [1] for Al, an initial specimen length of 6 mm and a strain of 0.02, the critical strain rate is found to be $\sim 0.1\ s^{-1}$. Since the thermal diffusivity of the composite is lower than the monolithic alloy, lower critical strain rates for the adiabatic heating of the composite is expected.

It has been found that particles that have sharp corners have higher strengthening effect in the composite than spherical particles [31]. The effect of sharp corners in the model was studied with the stress distribution in 15% spherical and cylindrical SiC-particulate reinforced model composites (Fig. 15a and b). At an average composite strain of 0.02, for example, the average matrix and particle stresses are 211 and 359 MPa for spherical particle, while these are 185 and 565 MPa for cylindrical particle. Development of the higher local stresses at the corner of the cylindrical particle is also clearly seen in Fig. 15b. The lower ductility and higher flow stresses in short fiber reinforced MMCs as compared with particulate reinforced MMCs are simply due to the development of the higher local stresses near to the reinforcement/matrix interface and higher load transfer to the reinforcement. Finally, the actual shape and the distribution of the reinforcement should however be taken into consideration when evaluating the effect of reinforcement on the strength of MMCs.

Previous numerical study has shown that particle clustering increases the plastic strains accumulated in the matrix, leading to a higher strain hardening and thus a higher flow stress [32]. Although the effect of particle clustering on the strain rate sensitivity of the composite has not been investigated yet, the development of higher plastic strains is expected to increase the constraint effect of the particles, which may lead to higher strain rate sensitivity.

During processing of the composite, the SiC particles may react with liquid Al, producing brittle Al-C phase and Si-rich region around the particle [33]. The Al-C phase is extremely brittle and it cannot be resolved under the electron microscope. The effect of brittle interface on the strain rate sensitivity is however not known very well.

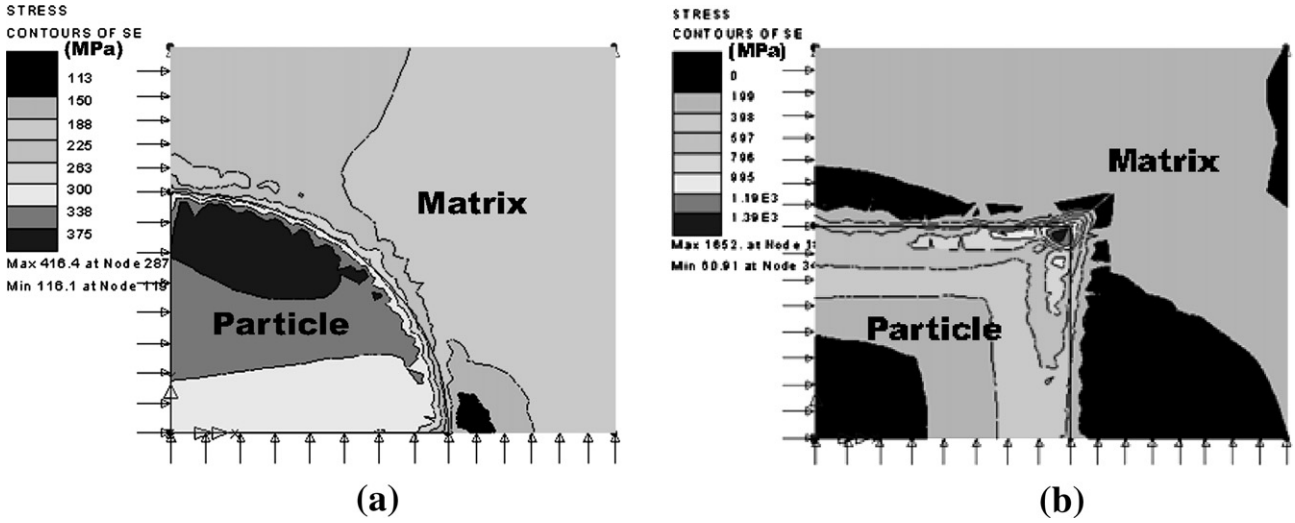

Fig. 15. Equivalent stress distribution at 0.02 average strain in a 15% SiC Al composite at1.5×10^{-3} s^{-1}: (a) spherical and (b) cylindrical particles.

As a summary, several parameters are considered for the discrepancy between experimental and numerical results. Among them, enhancement of the composite matrix microstructure, sharp corners and clustering of particles tend to increase flow stresses of the composite, while adiabatic heating and damage accumulation tend to decrease flow stress. The parameters that affect the strain rate sensitivity of the composite however should be further investigated through a systematical experimental research program that provides large number of data on composites of varying particle volume fractions and matrix alloys.

5. Conclusions

Strain rate dependent compression mechanical behavior of an SiC-particulate reinforced Al (2024-O) MMC with different particle volume fractions has been numerically investigated. An axisymmetric finite element unit cell model in which an elastic particle is embedded inside a strain rate sensitive viscoplastic matrix was used to determine composite stress–strain curves at various strain rates. The numerically calculated and experimentally found stress–strain curves and strain rate sensitivities were also compared for a 15% SiC particulate reinforced Al MMC. The following have been found based on numerical and experimental results:

1. The strain rate sensitivity of the composite was higher than that of the matrix. Strain rate sensitivity of the composite was further found to increase with increasing strain, although the matrix strain rate sensitivity was constant. This was attributed to the constrained effect of the particles.
2. Strain rate sensitivity of the composite increased with the increasing particle volume fraction at the same particle size. This was again attributed to the increased constrained effect of the particles with increasing particle volume fraction.
3. Although experimental strain rate sensitivity of 15% SiC reinforced MMC, increased with increasing strain (until 15% strain), it was found to be smaller than the numerical values. Several reasons for the discrepancy were discussed including assumption used in the model, adiabatic heating, microstructural variations between the composite matrix and matrix alloy, particle shape and distribution and damage accumulation.

References

[1] T.W. Clyne, P.J. Withers, An Introduction to Metal Matrix Composites, Cambridge University Press, 1993.
[2] M. Guden, I.W. Hall, J. Mater. Sci. 33 (1998) 3285.
[3] A.G. Evans, J.W. Hutchinson, R.M. McMeeking, Scripta Metall. 25 (1991) 3.
[4] J. Yang, S.M. Pickard, C. Cady, A.G. Evans, R. Mehrabbbian, Acta Metall. Mater. 39 (1991) 1863.
[5] W. Tong, G. Ravichandran, Compos. Sci. Technol. 52 (1994) 247.
[6] M. Dong, S. Schmauder, T. Bidlingmaier, A. Wanner, Comput. Mater. Sci. 9 (1997) 121.
[7] Y. Li, K.T. Ramesh, Acta Metal. Mater. 46 (1998) 5633.
[8] A.F. Whitehouse, T.W. Clyne, Acta Metal. Mater. 43 (1995) 2107.
[9] Y. Tomita, Y. Higa, T. Fujimoto, Int. J. Mech. Sci. 42 (2000) 2249.
[10] G. Bao, Z. Lin, Acta Metal. Mater. 44 (1996) 1011.
[11] G. Meijer, F. Ellyin, Z. Xia, Compos. Eng. Part B 31 (2000) 29.
[12] T. Christman, A. Needleman, S. Nutt, S. Suresh, Mater. Sci. Eng. A107 (1989) 49.
[13] J. Harding, M. Taya, in: Proc. 6th Int. Conf. On Composite Materials (ICCM VI) Elsevier Applied Science 3 (1987) 76.
[14] A. Marchand, J. Duffy, T.A. Christman, S. Suresh, Eng. Fract. Mech. 30 (1988) 295.
[15] C.C. Perng, J.R. Hwang, J.L. Doong, Mater. Sci. Eng. A171 (1993) 213.
[16] S.I. Hong, G.T. Gray III, J. Mater. Sci. 29 (1994) 2987.
[17] S. Yadav, D.R. Chichili, K.T. Ramesh, Acta Metal. Mater. 43 (1995) 4453.
[18] D.R. Chichili, K.T. Ramesh, Int. J. Solids Struct. 32 (1995) 2609.
[19] M. Güden, I.W. Hall, Mater. Sci. Eng. A242 (1998) 141.
[20] LUSAS, version 13, Theory Manual 1, United Kingdom.
[21] Y. Tirupataiah, G. Sundararajan, Mater. Sci. Eng. A189 (1994) 117.
[22] Y. Tirupataiah, Ph.D. Thesis, Banaras Hindu University, India, 1991.
[23] W.G. Ferguson, A. Kumar, J.E. Dorn, J. Appl. Phys. 38 (1967) 1836.

[24] G. Ravichandran, G. Subhash, J. Amer. Ceram. Soc. 77 (1994) 263.
[25] J. Lankford, Mater. Sci. Eng. A107 (1989) 261.
[26] F.J. Humpherys, 9th Rise Int. Symp. Mater. Sci. Riso National Lab. Roskilde, Denmark 51, 1988.
[27] J.J. Mason, A.J. Rosakis, G. Ravichandran, Mech. Mater. 17 (1994) 135.
[28] H.C. Rogers, Ann. Rev. Mat. Sci. 9 (1979) 283.
[29] C. Zener, J.H. Hollomon, J. Appl. Phys. 15 (1944) 22.
[30] M.A. Meyers, G. Subhash, B.K. Kad, L. Prasad, Mech. Mater. 17 (1994) 175.
[31] C.R. Chen, S.Y. Qin, S.X. Li, J.L. Wen, Mater. Sci. Eng. A278 (2000) 96.
[32] A. Borley, H. Biermann, O. Hartmann, Mater. Sci. Eng. A313 (2001) 34.
[33] F. Tongxiang, S. Zhongliang, Z. Di, V. Renjie, Mater. Sci. Eng. A257 (1998) 281.